Origin of open circuit voltage in planar and bulk heterojunction organic thin-film photovoltaics depending on doped transport layers

Christian Uhrich,[1,a)] David Wynands,[1] Selina Olthof,[1] Moritz K. Riede,[1] Karl Leo,[1] Stefan Sonntag,[2] Bert Maennig,[2] and Martin Pfeiffer[2]
[1]*Institut fuer Angewandte Photophysik, TU Dresden, Dresden, Germany*
[2]*Heliatek GmbH, D-01187 Dresden, Germany*

(Received 20 September 2007; accepted 25 June 2008; published online 29 August 2008)

The aim of this article is to investigate the origin of the open circuit voltage (V_{oc}) in organic heterojunction solar cells. The studied devices consist of buckminsterfullerene C_{60} as acceptor material and an oligophenyl-derivative 4,4′-bis-(*N*,*N*-diphenylamino)quaterphenyl (4P-TPD) as donor material. These photoactive materials are sandwiched between indium tin oxide and *p*-doped hole transport layers. Using two different *p*-doped hole transport layers, the built-in voltage of the solar cells is independently changed from the metal contacts. The influence of the built-in voltage on the V_{oc} is investigated in bulk and planar heterojunctions. In bulk heterojunctions, in which doped transport layers border directly on the photoactive blend layer, V_{oc} cannot exceed the built-in voltage significantly. Though, in planar heterojunctions, V_{oc} is identical with the splitting of quasi-Fermi levels at the donor-acceptor interface and is thus primarily determined by the difference of the lowest unoccupied molecular orbital of C_{60} and the highest occupied molecular orbital of 4P-TPD. In planar heterojunctions, the open circuit voltage can exceed the built-in voltage. Furthermore, the investigations show that the efficiency of organic solar cells can be improved by using *p*-doped charge transport layers with optimized energy level alignment to the active materials. The optimized planar heterojunction shows a fill factor of up to 65.5% and a V_{oc} of 0.95 V. For solar cells with insufficient energy level alignment between the photoactive layer system and the hole transport layer, a reduced V_{oc} in bulk heterojunction cells and a characteristic *S* shape of the *I-V* characteristics in planar heterojunction cells are observed. © *2008 American Institute of Physics*. [DOI: 10.1063/1.2973199]

I. INTRODUCTION

Organic solar cells are of great interest for future electrical power generation due to the prospects of low-cost production. They can be fabricated with a small amount of material, at low temperatures and on flexible cheap substrates. In 1986, Tang[1] presented the first efficient organic solar cell. Since then, efficiencies of up to 5% have been reached in small molecule photovoltaic cells.[2,3]

The power conversion efficiencies of solar cells are determined by the open circuit voltage V_{oc}, the fill factor (FF), and the short circuit current density J_{sc}.[4] Thus the physical understanding and optimization of V_{oc} plays an important role to increase solar cell efficiencies. In several publications, it was shown that in certain organic solar cell architectures V_{oc} scales with the difference of the lowest unoccupied molecular orbital (LUMO) of the acceptor material and the highest occupied molecular orbital (HOMO) of the donor material.[5–9] In this article, we show that in organic solar cells the origin of V_{oc} depends strongly on the cell architecture. It can either be primarily determined by the built-in potential V_{bi} or the difference of energy levels of donor and acceptor materials.

In the here presented solar cells, the photoactive materials are sandwiched between an indium tin oxide (ITO) contact and *p*-doped hole transport layers (HTLs).[10] In our devices, we define the built-in potential $e \cdot V_{bi}$ to be the difference in work functions (WFs) of the ITO contact and the *p*-doped HTL.

To investigate the influence of the built-in potential on V_{oc} and FF, small molecule solar cells in bulk heterojunction (BHJ) architecture and planar heterojunctions (PHJs) were prepared each with two different doped HTLs. Using these HTLs, V_{bi} can be tuned independently of the WF of the metal electrodes.[11]

In order to interpret the experimental findings, we will first briefly discuss the transport of charge carriers in solar cells: in photovoltaic cells, the photogenerated free charge carriers are transported to the contacts by (i) the electric field $E(x)$ and (ii) diffusion due to a charge carrier concentration gradient. Following Ref. 12 the current density in one-dimension of electrons $J_n(x)$ can be expressed as

$$J_n(x) = en(x)\mu_n E(x) + kT\mu_n \nabla n(x), \tag{1}$$

where $n(x)$ is the concentration of charge carriers, μ_n is the electron mobility, $E(x)$ is the electric field, k is Boltzmann's constant, and T is the absolute temperature. Equation (1) was derived under the assumption that the Einstein relation[13] holds.[14,15] At high carrier densities deviations from the Einstein relation can occur.[16]

Alternatively, the sum of drift and diffusion current can be expressed in terms of the gradient in the quasi-Fermi level for electrons $\nabla E_{Fn}(x)$:[17,18]

[a)]Electronic mail: christian.uhrich@iapp.de.

$$J_n(x) = n(x)\mu_n \nabla E_{\mathbf{Fn}}(x) \tag{2}$$

and analog for holes.

When no gradient in the quasi-Fermi levels is present or the electron flux cancels the hole flux, the net current flow is zero[14] and the applied voltage corresponds to V_{oc}. Assuming Ohmic contacts to the electrodes, V_{oc} can be expressed in the following way:

$$eV_{oc} = E_{\mathbf{Fn},x=0} - E_{\mathbf{Fp},x=d}, \tag{3}$$

where $x=0$ is the position of the electron contact and $x=d$ the hole contact. If the quasi-Fermi levels are constant from the region of photogeneration to the corresponding contacts, V_{oc} becomes maximal and equals the maximum splitting of quasi-Fermi levels anywhere in the solar cell.[14] With the definition of quasi-Fermi levels in classical semiconductor physics applied on organic disordered systems, the maximal V_{oc} can be expressed in the following way:

$$eV_{oc,\max} = E_{\mathbf{LUMO},A} - E_{\mathbf{HOMO},D} - kT \ln \frac{N_{\mathbf{LUMO},A} N_{\mathbf{HOMO},D}}{np}, \tag{4}$$

where $E_{\mathbf{LUMO},A}$ is the energetic position of the LUMO of the acceptor (A) and $E_{\mathbf{HOMO},D}$ the energetic position of the HOMO of the donor (D). $N_{\mathbf{LUMO},A}$ is the density of states of the LUMO of the acceptor and $N_{\mathbf{HOMO},D}$ the density of states of the HOMO of the donor, n is the density of electrons of the acceptor and p the density of holes of the donor.

For simplification, it was assumed that charge carrier transport takes place only on one level corresponding to HOMO and LUMO, respectively.

II. EXPERIMENTAL

Organic photovoltaic cells were prepared, using buckminsterfullerene C_{60} as acceptor and 4,4′-bis-(*N*,*N*-diphenylamino)quaterphenyl (4P-TPD) as donor. These photoactive materials were sandwiched between ITO and a *p*-doped HTL. As HTL we used *N*,*N*,*N*′,*N*′-tetrakis(4-methoxyphenyl)benzidine (MeO-TPD) and *N*,*N*′-diphenyl-*N*,*N*′-bis(4′-(*N*,*N*-bis(naphth-1-yl)-amino)-biphenyl-4-yl) benzidine (DiNPD). Both HTLs were *p*-doped by tetrafluoro-tetracyano-quinodimethane (F_4-TCNQ) prepared by coevaporation. A thin layer of Zn-phthalocyanine (ZnPc) doped by F_4-TCNQ ensures an Ohmic contact between the organics and metal top contact.[10] The molecular structures of the used materials are shown in Fig. 1. C_{60} and ZnPc were provided by Alfa Aesar, 4P-TPD, DiNPD, and MeO-TPD by Sensient Imaging Technologies and F_4-TCNQ by Aldrich. All materials were purified at least once by gradient sublimation.

To prepare the organic photovoltaic cells, glass substrates covered with a layer of 120 nm ITO with a sheet resistance of $<30\ \Omega/SQ$ were used (Thin Film Devices Inc.). The ITO was patterned such so that three solar cells with an area of approximately 3 mm^2 were obtained on each substrate. Prior to the deposition of the organic thin films, the substrates were cleaned in an ultrasonic bath of a detergent, acetone, and ethanol. No plasma treatment was used.

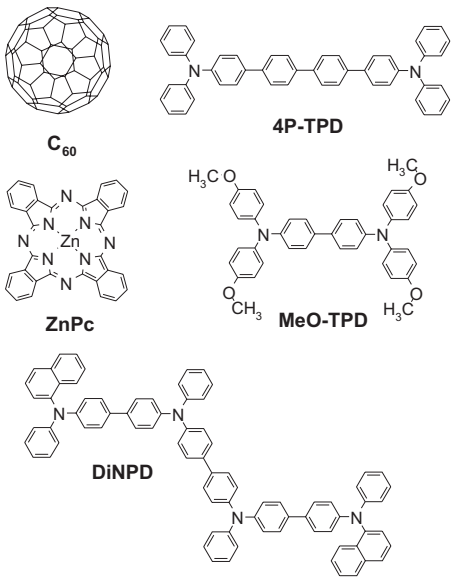

FIG. 1. Chemical structures of the organic materials. Fullerene C_{60} is used as acceptor material and 4P-TPD is used as donor material. In the presented devices, either MeO-TPD or DiNPD are used as hole transport material *p*-doped with F_4-TCNQ. A thin zinc-phthalocyanine layer doped with F_4-TCNQ is used as contact layer between HTL and metal contact.

All organic layers and the metal contacts were thermally deposited in a high vacuum system (base pressure 2×10^{-7} mbar) through shadow masks onto the precleaned ITO substrates without breaking the vacuum. All measurements were carried out using a Source Measurement Unit 236 SMU from Keithley in a N_2-filled glovebox without exposing the samples to air. Illumination was provided by a sun simulator with an average intensity of 127 mW/cm^2, as determined by a silicon reference cell (Fraunhofer Institute for Solar Energy Systems ISE, Germany). The mismatch between the spectrum of our sun simulator and AM1.5 spectrum was not taken into account when calculating the power conversion efficiencies of the solar cells.

We prepared BHJ solar cells with a donor-acceptor blend of C_{60} and 4P-TPD and PHJ solar cells with pristine layers of C_{60} and 4P-TPD. Each type of solar cell architecture was prepared with MeO-TPD and DiNPD as HTL. The corresponding cell architectures are shown in Fig. 2.

The BHJ solar cells [Fig. 2(I)] are prepared in the following layer sequence: glass/ ITO/ 5 nm C_{60}/30 nm C_{60}:4P-TPD (3:1)/ 5 nm HTL/ 20 nm *p*-HTL/10 nm *p*-ZnPc/10 nm Au/ 100 nm Al. F_4-TCNQ is used as *p*-dopant with a doping ratio of 2.5 mol % in MeO-TPD and ZnPc and with a doping ratio of 7 mol % in DiNPD.

MeO-TPD is used as HTL in sample **A** and DiNPD in

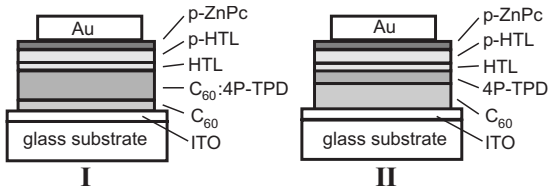

FIG. 2. BHJ solar cell architecture of samples **A** and **B** (I), and PHJ architecture of samples **C** and **D** (II).

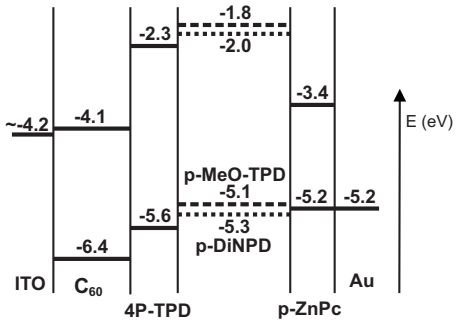

FIG. 3. Energy levels of the used materials with respect to the vacuum level. The values for C_{60}, 4P-TPD, DiNPD, MeO-TPD and ZnPc were measured by UPS, the value of ITO was taken from literature (Ref. 21). The LUMO of C_{60} is calculated from the HOMO and the energy gap of 2.3 eV measured by photoelectron and inverse-photoelectron spectroscopy (Ref. 20).

sample **B**. The C_{60}:4P-TPD-blend layer is deposited on a heated substrate (~100 °C) to improve the cell's FF. Under these conditions, the blend layer grows in a more crystalline morphology, which leads to an improvement of percolation paths and thus to an improvement in the charge carrier mobility.[19]

Using the same materials, PHJs [Fig. 2(II)] are prepared with the layer sequence: glass/ITO/30 nm C_{60}/17.5 nm 4P-TPD/5 nm HTL/20 nm *p*-HTL/10 nm *p*-ZnPc/10 nm Au/ 100 nm Al. Again, MeO-TPD was used as HTL in sample **C** and DiNPD in sample **D** with the same doping ratios of samples **A** and **B**.

Figure 3 shows the energy levels of the materials used with respect to the vacuum level. The ionization potentials (IPs) of all organic materials were measured by ultraviolet-photoelectron spectroscopy (UPS) with an energy resolution of 150 meV. The values of the IP are: C_{60} 6.4 eV, 4P-TPD 5.6 eV, *p*-doped MeO-TPD 5.1 eV, *p*-doped DiNPB 5.3 eV, and *p*-doped ZnPc 5.2 eV. The LUMO positions of 4P-TPD (−2.3 eV), DiNPB (−2.0 eV), ZnPc (−3.4 eV), and MeO-TPD (−1.8 eV) were estimated by taking the IP and adding the optical gap using the low energy cutoff of the thin-film absorption spectra. To account for the exciton binding energy another 0.3 eV were added to this value. 4P-TPD has a large band gap of about 3.3 eV and is therefore marginally contributing to the current of the solar cells. The electron affinity of C_{60} (−4.1 eV) was calculated from the IP and a band gap of 2.3 eV.[20]

To estimate V_{bi}, the WFs of C_{60}, *p*-doped MeO-TPD and *p*-doped DiNPB were also measured with UPS. In this paper, we define $e \cdot V_{bi}$ to be the difference of the WFs of C_{60} and the doped HTL. Provided that no interface dipoles are present between the organic layers, a bias of V_{bi} corresponds to flatband situation in the devices.

The measurement yields a WF for a 10 nm thin C_{60} layer on ITO of 4.2 eV. For the *p*-side, a 10 nm thin layer of ZnPc doped with F4-TCNQ (2.5 mol %) was deposited on a gold substrate. Onto this, 5 nm of the doped HTL was evaporated and analyzed with UPS. The resulting WF of *p*-doped MeO-TPD (2.5 mol %) is 4.7 eV. In addition the WF of *p*-doped DiNPB (7 mol %) is 4.9 eV. From these values we calculate

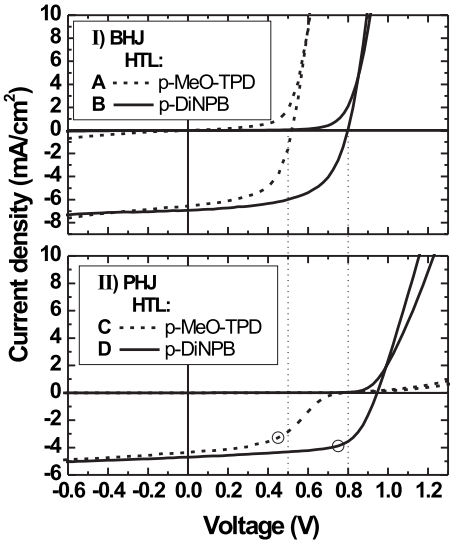

FIG. 4. *I-V* characteristics of *M-i-p* type heterojunctions under 127 mW/cm^2 simulated sun light. (I) BHJ solar cells with the layer sequence ITO/ 5 nm C_{60}/30 nm C_{60}:4P-TPD (3:1)/ 5 nm HTL/ 20 nm *p*-HTL/10 nm *p*-ZnPc/10 nm Au/ 100 nm Al. The HTL is: sample **A** MeO-TPD; **B** DiNPD. The substrate has been heated (~100 °C) while blend layer deposition. (II) PHJ solar cells with the layer sequence ITO/ 30 nm C_{60}/17.5 nm 4P-TPD/ 5 nm HTL/ 20 nm *p*-HTL/10 nm *p*-ZnPc/10 nm Au/ 100 nm Al. The HTL is: sample **C** MeO-TPD; **D** DiNPD. The dotted lines mark V_{bi} in the respective solar cells. The open circles represent the maximum power point in the PHJ.

a V_{bi} of 0.5 V for our devices using *p*-doped MeO-TPD as HTL (samples **A** and **C**) and 0.7 V for the devices with *p*-doped DiNPB (samples **B** and **D**).

III. RESULTS AND DISCUSSION

In Fig. 4, the *I-V* characteristics of the four samples under illumination are plotted. All corresponding values of samples **A**,**B**,**C**, and **D** are given in Table I.

A. Bulk heterojunction solar cells

In Fig. 4(I), the *I-V* characteristics of the BHJ solar cells **A** and **B** are depicted. The dashed line shows the performance of the BHJ **A**, comprising MeO-TPD as HTL. J_{sc} is 6.57 mA/cm^2, V_{oc} is 0.52 V, and the FF is 58.3%. The *I-V* curve was measured at a light intensity of 127 mW/cm^2. The power conversion efficiency η is 1.57% (mismatch to AM1.5 was not corrected). The large gap of the donor mate-

TABLE I. BHJ and PHJ solar cells with MeO-TPD and DiNPD as HTL, respectively. The column "arch" names the architecture of the solar cell. Illumination is provided by a sun simulator (127 mW/cm^2) referenced with a Si diode. Mismatch to AM1.5 was not corrected.

Sample	Arch	HTL	J_{sc} (mA/cm^2)	V_{oc} (*V*)	FF (%)	η (%)
A	BHJ	MeO	6.57	0.52	58.3	1.57
B	BHJ	DiNPD	6.94	0.80	58.4	2.55
C	PHJ	MeO	4.35	0.78	43.5	1.16
D	PHJ	DiNPD	4.70	0.95	65.5	2.30

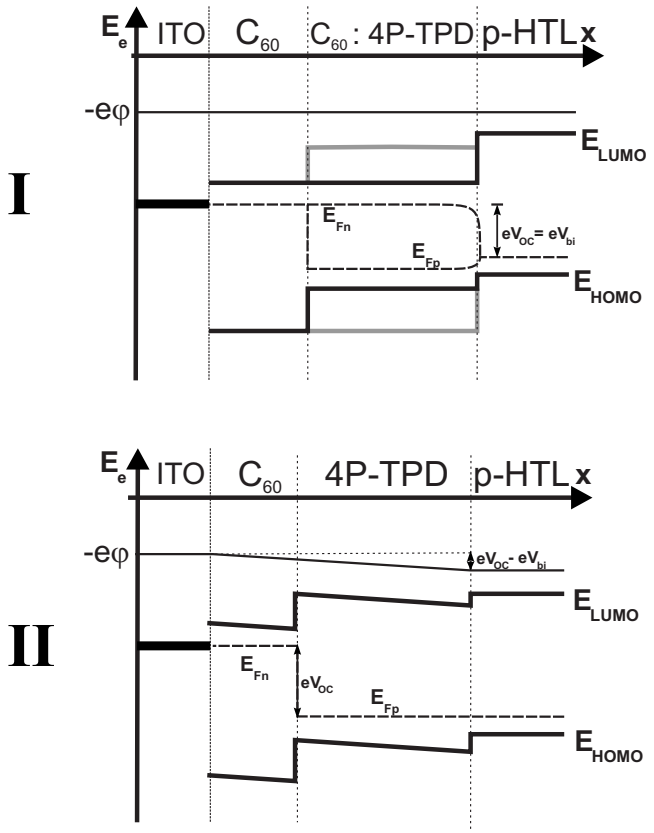

FIG. 5. Potential curves in a BHJ (I) and a PHJ (II) photovoltaic cell under open circuit conditions. (I) The layer sequence of the BHJ is: ITO / C_{60} (acceptor) / C_{60}:4P-TPD (acceptor donor blend) / *p*-doped HTL (either MeO-TPD or DiNPD). In the blend layer (C_{60}:4P-TPD), $E_{\mathbf{LUMO}}$ is the LUMO of the acceptor and $E_{\mathbf{HOMO}}$ the HOMO of the donor material. The HOMO level of the HTL is energetically higher compared to the donor material. The open circuit voltage times *e* corresponds to the difference of quasi-Fermi level for electrons $E_{\mathbf{Fn}}$ in the C_{60} layer and the quasi-Fermi level for holes $E_{\mathbf{Fp}}$ in the *p*-HTL. This difference is smaller compared to the maximum splitting of quasi-Fermi levels in the blend layer. (II) The layer sequence of the PHJ is: ITO / C_{60} (acceptor) / 4P-TPD (donor) / *p*-doped HTL (either MeO-TPD or DiNPD). Free charge carriers are generated at the interface of C_{60} and 4P-TPD. The difference of $E_{\mathbf{Fn}}$ in the C_{60} layer and $E_{\mathbf{Fp}}$ in *p*-HTL corresponding to eV_{oc} is identical with the splitting of quasi-Fermi levels at the donor-acceptor interface.

rial (4P-TPD) of about 3.3 eV in combination with the comparably high J_{sc} indicates a mismatch of our sun simulator resulting in an overestimation of η.

In Fig. 4(I), the solid line shows the *I-V* characteristics of the BHJ solar cell **B**. The layer sequence of **B** is identical to that of **A** except for the HTL. In **B**, the HTL is DiNPD. The sample shows a J_{sc} of 6.94 mA/cm^2, V_{oc} of 0.80 V, a FF of 58.4%, leading to η of 2.55% at 127 mW/cm^2.

The short circuit current of devices **A** and **B** are comparable. We conclude that the exchange of the HTL has only a small influence on the optical field distribution, the absorption of light in the photoactive materials, the generation of charge carriers at the interface, and the charge collection efficiency.

However, the open circuit voltage is increased by 0.28 V by changing the *p*-doped HTL from MeO-TPD to DiNPD.

In the following, we will discuss the increase in V_{oc} in the presented BHJs in terms of potential curves and splitting of quasi-Fermi levels. In Fig. 5, the simplified energy diagram of the bulk and PHJs under V_{oc} conditions are shown. Figure 5(I) shows the potential curves of the BHJs. In the simplified picture, the energy levels of the acceptor (C_{60}), the photoactive blend layer (C_{60}:4P-TPD), and the doped HTL are depicted. The thin intrinsic HTL is not shown in this picture. Charge carriers are generated throughout the C_{60}:4P-TPD blend leading to a splitting of the quasi-Fermi levels $E_{\mathbf{Fn}}$ and $E_{\mathbf{Fp}}$. There, $E_{\mathbf{LUMO}}$ is the LUMO of the acceptor (C_{60}) and $E_{\mathbf{HOMO}}$ the HOMO of the donor material (4P-TPD). In the volume of the pristine C_{60} layer and the *p*-HTLs, no free charge carriers are generated, such that minority carriers do not play a role. Electrons can leave the photoactive blend layer through the pristine C_{60} layer, whereas holes are blocked at the interface to C_{60}. Holes can leave the blend layer through the *p*-HTL and are blocked at the interface to the pristine C_{60} layer.

The difference between the quasi-Fermi level for electrons $E_{\mathbf{Fn}}$ in the C_{60} layer and the quasi-Fermi level for holes $E_{\mathbf{Fp}}$ in the HTL is identical to eV_{oc} if no charge carrier transport to the contacts takes place. As stated above, the generation of free charge carriers in samples **A** and **B** are the same. Thus, the maximum splitting of the quasi-Fermi levels has to be similar in both samples.

Experimentally, we find a V_{oc} of about 0.5 V in sample **A** and a V_{oc} of 0.8 V in sample **B**.

Accordingly in sample **A**, the difference of quasi-Fermi levels at the contacts is reduced compared to the maximum splitting of the quasi-Fermi levels in the photoactive bulk. In Fig. 5(I), this behavior is represented by the convergence of $E_{\mathbf{Fn}}$ and $E_{\mathbf{Fp}}$ in the blend layer close to the *p*-HTL.

Furthermore, in the solar cell architectures of samples **A** and **B**, the open circuit voltage cannot exceed the built-in voltage significantly. Assuming no level bending in the intrinsic layers, the electric field *E* in the undoped organic layers supporting the transport of photogenerated charge carriers vanishes if a bias of V_{bi} is applied. Due to the Ohmic contacts, charge carriers are injected from the contacts into the organic layers at bias above V_{bi}. Injected holes are transported barrier free to the interface of the *p*-HTL and the blend layer, where they recombine with injected electrons from the C_{60} layer. The recombination current of injected charge carriers exceeds the current of photo generated charge carriers, such that the applied voltage has already exceeded V_{oc}. Therefore in the BHJ as depicted in Fig. 5(I), V_{oc} cannot exceed V_{bi} significantly.

Thus, V_{bi} is approximately 0.5 V in the here presented solar cells comprising *p*-MeO-TPD as *p*-HTL and approximately 0.8 V in the solar cells incorporating *p*-DiNPD as *p*-HTL. These values correspond within the margins of error with the values determined from UPS measurements discussed earlier in this work (0.5 V and 0.7 V). The significant increase of V_{oc} by about 0.3 V compared to the sample with *p*-MeO-TPD can thus be clearly attributed to the increased V_{bi} in these samples, which is caused by the higher IP of DiNPD and the higher doping ratios leading to an increased WF of the doped HTL. This observation in turn confirms that V_{oc} of sample **A** was indeed limited by the low V_{bi}, rather than by the quasi-Fermi level splitting in the photoactive layer system.

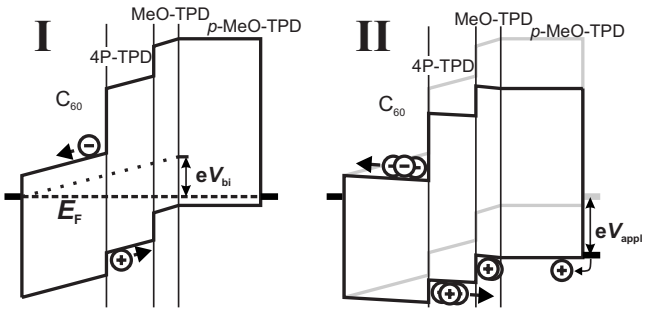

FIG. 6. Energy levels of PHJ sample **C** with MeO-TPD as HTL. (I) Energy levels under short circuit conditions. eV_{bi} drops over the intrinsic layers. Photogenerated charge carriers are transported by electric field (drift) and diffusion to the contacts. (II) A voltage close to V_{oc} is applied. The effective electric field counteracts the flow of photo generated charge carriers to the contacts. Holes injected from the contact pile up at the MeO-TPD/ 4P-TPD barrier. The recombination of injected charge carriers is hindered. The *I-V* characteristics are thus *S*-shaped. The gray lines depict the energy levels under short circuit conditions.

B. Planar heterojunction photovoltaic cells

Figure 4(II) shows the *I-V* characteristics of the PHJ solar cells **C** and **D**.

In Fig. 4(II), the dashed line shows the performance of the solar cell with MeO-TPD as HTL (sample **C**). The sample exhibits a J_{sc} of 4.35 mA/cm^2, a V_{oc} of 0.78 V, a FF of 43.5%, and a η of 1.16% (127 mW/cm^2). The most prominent features of sample **C** are the low FF and the increase of V_{oc} compared to sample **A**.

First the low FF will be discussed: In the voltage range from 0.7 to 0.9 V, the current density of sample **C** is very low resulting in a *S*-shaped *I-V* characteristics and the low FF. This *S*-shape is a phenomenon occasionally observed in organic photovoltaic cells.[22,23] Figure 6 schematically shows the energy levels of PHJ **C**. Figure 6(I) represents the short circuit situation, while in 6 (II) the bias is increased to a voltage slightly above V_{bi} (0.5 V). When no voltage is applied, charge carriers generated at the C_{60}/4P-TPD interface are driven to the contacts by the electric field $E(x)$ and the concentration gradient of free charge carriers $\nabla n(x)$ (Eq. (1)). The charge carrier transport to the contacts is barrier free.

By increasing the applied voltage such that it is slightly higher than V_{bi} (0.5 V), the electric field E in the intrinsic layers counteracts the flow of photogenerated charge carriers [Fig. 6(II)]. The free charge carriers are driven to the contacts by diffusion against the electric field [Eq. (1)]. To drive a current, an electron concentration gradient has to built up in the C_{60} layer and a hole concentration gradient in the 4P-TPD layer. Consequently, the number of electrons and holes at the donor-acceptor interface increases significantly. As a result, the recombination of electrons and holes at the donor-acceptor interface is enhanced and a significant drop in the photocurrent is detected at a bias of around 0.5 V (V_{bi}).

Accordingly, the flow of photogenerated charge carriers becomes very small in the voltage range between 0.7 and 0.8 V. Simultaneously, holes are injected through the gold contact on the HOMO of MeO-TPD [Fig. 6(II)]. These holes pile up at the MeO-TPD/4P-TPD-interface because they are blocked by an energetic barrier of about 0.5 eV. The recombination of injected holes with electrons on the LUMO of C_{60} is suppressed. Neither a forward nor a photocurrent occurs in a relatively wide voltage range (0.7–0.9 V).

At higher applied voltages, injected holes can overcome the MeO-TPD/4P-TPD-barrier. The holes on 4P-TPD can recombine with electrons on C_{60} so that a current in forward direction flows. These transport dynamics of charge carriers manifest as an *S*-shape in the *I-V* characteristics.

The solid line in Fig. 4(II) displays the *I-V* characteristics of the PHJ solar cell with DiNPD as HTL (sample **D**). The sample shows a J_{sc} of 4.70 mA/cm^2 and V_{oc} of 0.95 V (127 mW/cm^2). The solar cell has a very high FF of 65.5% being one of the highest FF observed for organic small molecule solar cells. The *I-V* characteristics do not show any *S*-shape. In contrast to sample **C**, the electric field E still supports the flow of photo generated charge carriers at an applied voltage of 0.5 V due to the increase in V_{bi} to 0.8 V (0.7 eV from UPS) in samples with DiNPD as HTL. Thus the high FF was achieved. Second, the exchange of the HTL leads to a reduction in the barrier height in the HOMO level between the HTL and 4P-TPD. Thus, the recombination of injected charge carriers at bias higher V_{oc} is not hindered by a high energetic barrier between the HTL and the 4P-TPD layer. Consequently, the increase in the current at applied voltages higher than V_{oc} is much steeper compared to sample **C**.

In the following, we will construct the potential curves for the PHJ (sample **C** and **D**): Fig. 5(II) shows the potential curves under V_{oc} of the PHJ structures. The figure shows the intrinsic C_{60} layer, the 4P-TPD layer, and the *p*-doped HTL analogical to the discussion of the BHJs.

In contrast to BHJ, photogenerated excitons are dissociated into free electrons in the C_{60} layer and free holes in the 4P-TPD layer only at the interface between C_{60} and 4P-TPD. In the volume of the C_{60}, 4P-TPD, and *p*-doped HTL, no free charge carriers are photogenerated, such that minority carriers do not play a role. In the figure, the quasi-Fermi levels are constant, indicating that no charge carrier transport is taking place. Recombination of charge carriers primarily takes place at the donor-acceptor interface. Consequently, the quasi-Fermi levels at the contacts are identical with the related quasi-Fermi levels at the exciton dissociating interface if the bias equals V_{oc}. Thus Eq. (4) is valid. Furthermore, the energetic barrier in the HOMO level between the *p*-HTL and 4P-TPD prevents the recombination of injected charge carriers. Thus, in PHJ, V_{oc} can exceed the built-in voltage if the illumination is sufficiently high and E_g is significantly larger than V_{bi}. In that case under open circuit conditions, the electric field in the intrinsic layers is reversed as compared to short circuit conditions. The electric field counteracts the diffusion of photo generated charge carriers away from the photoactive interface.

Comparing PHJs **D** and **C**, V_{oc} increases by 0.17 V, although Eq. (4) is valid and $E_{\mathbf{LUMO},A} - E_{\mathbf{HOMO},D}$ is equivalent in both of the samples. Additionally, the number of photogenerated excitons in both of the samples is identical, indicated by the equivalent short circuit current in both PHJs. However, upon approaching V_{oc}, the higher V_{bi} of samples **D** supports exciton separation and counteracts interface carrier recombination more effectively in contrast to sample **C** with

a lower V_{bi}. Thus at the same bias, the number of free charge carriers is enhanced in **D** compared to **C**. This does not only lead to higher photocurrents close to V_{oc}, but according to Eq. (4) also to a slight increase of V_{oc}.

C. Comparing BHJ and PHJ

Earlier, we compared two BHJs (samples **A** and **B**) and then two PHJs (samples **C** and **D**). In the following, we will directly compare samples with different structures and the same HTL.

Comparing PHJs (samples **C** and **D**) and BHJs (samples **A** and **B**), the BHJ solar cells show an increase of about 2 mA/cm^2 in short circuit current. By blending the acceptor material C_{60} with the donor material 4P-TPD, the dimension of the donor-acceptor interface is enhanced. More excitons can reach the exciton separating interface and can thus be dissociated into free charge carriers such that J_{sc} increases.

Comparing the FFs of BHJ **A** and PHJ **C**, FF decreases from 58.3% to 43.5%. This can most likely be attributed to the *S*-shaped curvature of sample **C**.

However, the FF of PHJ **D** (65.5%) is significantly larger compared to BHJ **B** (58.3%). This might be attributed to the spatial separation of positive and negative charge carriers at the donor-acceptor interface in PHJs. First, the spatial separation leads to a high charge carrier concentration gradient supporting the transport of charge carriers. Second, in PHJ recombination of charge carriers only takes place at the donor-acceptor interface. Additionally, charge carrier mobilities are strongly reduced in donor-acceptor blend layers compared to the mobilities in the pristine materials.[19]

As discussed before, the open circuit voltage in our BHJ is primarily determined by the built-in voltage. In PHJ, V_{oc} equals the splitting of quasi-Fermi levels at the donor-acceptor interface and is thus primarily by $E_{\mathbf{LUMO},A} - E_{\mathbf{HOMO},D}$. Comparing BHJ **A** and PHJ **C** both incorporating MeO-TPD as HTL, one finds an increase in V_{oc} from 0.52 to 0.78 V. Comparing BHJ **B** and PHJ **D** incorporating DiNPD as HTL, V_{oc} increases from 0.80 to 0.95 V.

Hence the open circuit voltage in BHJ corresponds approximately the value of V_{bi} in solar cells incorporating the same transport layers, it has direct influence on the transport of charge carriers in PHJ. Interestingly, V_{oc} of BHJ **A** (0.52 V) is close to the bias of PHJ **C** at the maximum power point (0.45 V). The same is true for the samples incorporating DiNPD as HTL: V_{oc} of BHJ **B** (0.80 V) is close to the voltage of PHJ **D** at the maximum power point (0.75 V). In Fig. 4 the position of the maximum power point is shown as circle in the *I-V* characteristics.

IV. CONCLUSION

We have investigated the influence of various parameters on the open circuit voltage in small molecule organic solar cells. We used different *p*-doped HTLs, MeO-TPD and DiNPD with different WFs leading to a change in the built-in potentials V_{bi} of the cells. We find that V_{bi} has a strong and direct influence on V_{oc} for BHJ solar cells. The influence of V_{bi} on V_{oc} is less pronounced for PHJs. Here, however, we find a characteristic *S*-shape of the *I-V* characteristics, if V_{oc} significantly exceeds V_{bi}. We interpret our results via splitting of quasi-Fermi levels and show a fundamental difference in planar and BHJs. The *S*-shaped *I-V* characteristics are interpreted in terms of driving forces that act on charge carriers and energetic barriers within the device.

For a PHJ sample with optimized level alignment between the doped HTL and the photoactive system, we achieved a FF of 65.5% and V_{oc} of 0.95 V (127 mW/cm^2). To achieve high power conversion efficiencies, the wide-gap model donor 4P-TPD used in this study needs to be replaced by a strongly absorbing donor material.

ACKNOWLEDGMENTS

We thank the German Federal Ministry for Education and Research BMBF (network Project No. 01SF0119) and the Deutsche Forschungsgemeinschaft (Leibniz prize) for financial support.

[1] C. W. Tang, Appl. Phys. Lett. **48**, 183 (1986).
[2] J. G. Xue, B. P. Rand, S. Uchida, and S. R. Forrest, Adv. Mater. (Weinheim, Ger.) **17**, 66 (2005).
[3] J. G. Xue, B. P. Rand, S. Uchida, and S. R. Forrest, J. Appl. Phys. **98**, 124903 (2005).
[4] P. Peumans, A. Yakimov, and S. R. Forrest, J. Appl. Phys. **93**, 3693 (2003).
[5] C. J. Brabec, A. Cravino, D. Meissner, N. S. Sariciftci, T. Fromherz, M. T. Rispens, L. Sanchez, and J. C. Hummelen, Adv. Funct. Mater. **11**, 374 (2001).
[6] L. J. A. Koster, V. D. Mihailetchi, and P. W. M. Blom, Appl. Phys. Lett. **88**, 093511 (2006).
[7] M. C. Scharber, D. Wuhlbacher, M. Koppe, P. Denk, C. Waldauf, A. J. Heeger, and C. J. Brabec, Adv. Mater. (Weinheim, Ger.) **18**, 789 (2006).
[8] B. P. Rand, D. P. Burk, and S. R. Forrest, Phys. Rev. B **75**, 115327 (2007).
[9] C. Uhrich, R. Schueppel, A. Petrich, K. Leo, M. Pfeiffer, E. Brier, P. Kilickiran, E. Reinold, and P. Baeuerle, Adv. Funct. Mater. **17**, 2991 (2007).
[10] J. Drechsel, B. Maennig, D. Gebeyehu, M. Pfeiffer, K. Leo, and H. Hoppe, Org. Electron. **5**, 175 (2004).
[11] K. Schulze, B. Maennig, Y. Tomita, C. May, J. Huepkes, E. Brier, E. Reinold, P. Baeuerle, and K. Leo, Appl. Phys. Lett. **91**, 073521 (2007).
[12] A. L. Fahrenbruch and R. H. Bube, *Fundamentals of Solar Cells: Photovoltaic Solar Energy Conversion* (Academic, New York, 1983).
[13] B. Sapoval and C. Hermann, *Physics of Semiconductors* (Springer-Verlag, New York, 2003).
[14] B. A. Gregg, J. Phys. Chem. B **107**, 4688 (2003).
[15] L. J. A. Koster, E. C. P. Smits, V. D. Mihailetchi, and P. W. M. Blom, Phys. Rev. B **72**, 085205 (2005).
[16] Y. Roichman and N. Tessler, Appl. Phys. Lett. **80**, 1948 (2002).
[17] P. Wuerfel, *Physics of Solar Cells: From Principles to New Concepts* (Wiley, Weinheim, 2005).
[18] B. A. Gregg and M. C. Hanna, J. Appl. Phys. **93**, 3605 (2003).
[19] A. Opitz, M. Bronner, and W. Brutting, J. Appl. Phys. **101**, 063709 (2007).
[20] R. W. Lof, M. A. Vanveenendaal, B. Koopmans, H. T. Jonkman, and G. A. Sawatzky, Phys. Rev. Lett. **68**, 3924 (1992).
[21] J. S. Kim, M. Granstrom, R. H. Friend, N. Johansson, W. R. Salaneck, R. Daik, W. J. Feast, and F. Cacialli, J. Appl. Phys. **84**, 6859 (1998).
[22] M. Glatthaar, M. Riede, N. Keegan, K. Sylvester-Hvid, B. Zimmermann, M. Niggemann, A. Hinsch, and A. Gombert, Sol. Energy Mater. Sol. Cells **91**, 390 (2007).
[23] K. Schulze, C. Uhrich, R. Schueppel, K. Leo, M. Pfeiffer, E. Brier, E. Reinold, and P. Baeuerle, Adv. Mater. (Weinheim, Ger.) **18**, 2872 (2006).